

Context-Guided Spatial Feature Reconstruction for Efficient Semantic Segmentation

Zhenliang Ni, Xinghao Chen^(✉), Yingjie Zhai, Yehui Tang, and Yunhe Wang^(✉)

Huawei Noah's Ark Lab
{xinghao.chen, yunhe.wang}@huawei.com

Abstract. Semantic segmentation is an important task for many applications but it is still quite challenging to achieve advanced performance with limited computational costs. In this paper, we present CGRSeg, an efficient yet competitive segmentation framework based on context-guided spatial feature reconstruction. A Rectangular Self-Calibration Module is carefully designed for spatial feature reconstruction and pyramid context extraction. It captures the global context in both horizontal and vertical directions and gets the axial global context to explicitly model rectangular key areas. A shape self-calibration function is designed to make the key areas more close to the foreground object. Besides, a lightweight Dynamic Prototype Guided head is proposed to improve the classification of foreground objects by explicit class embedding. Our CGRSeg is extensively evaluated on ADE20K, COCO-Stuff, and Pascal Context benchmarks, and achieves state-of-the-art semantic performance. Specifically, it achieves 43.6% mIoU on ADE20K with only 4.0 GFLOPs, which is 0.9% and 2.5% mIoU better than SeaFormer and SegNeXt but with about 38.0% fewer GFLOPs. Code is available at <https://github.com/nizhenliang/CGRSeg>.

Keywords: Pyramid Context · Spatial Feature Reconstruction · Rectangular Self-Calibration

1 Introduction

Semantic segmentation is a foundational computer vision task that aims to assign semantic labels to each pixel in an image. In recent years, deep learning methods have achieved remarkable results in semantic segmentation, thanks to the availability of large-scale datasets, powerful computing resources, and advanced network architectures. Early studies for semantic segmentation are mainly based on convolution neural networks (CNNs), such as FCN [23], PSPNet [36], and DeepLab [4–6, 21]. More recently, a series of methods for semantic segmentation have been proposed based on vision transformer and achieve competitive performance [25, 28, 33, 37]. Deep learning based methods have significantly improved the accuracy of semantic segmentation. However, it is still a quite challenging

✉ Corresponding authors.

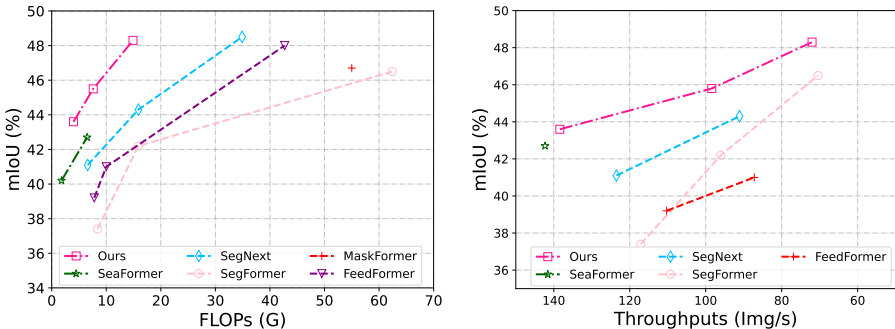


Fig. 1: Performance vs. FLOPs and Throughput on ADE20K [38]. Our model achieves better trade-off between accuracy and computational cost than prior methods. Moreover, our model outperforms other models in throughput with higher accuracy.

topic for how to achieve advanced segmentation performance with limited computing resources.

Efficient and lightweight semantic segmentation is an important topic and has attracted great research interest. Yu *et al.* [29] proposed BiSeNet, which is a two-pathway architecture to capture local and global information and achieves a good balance between speed and segmentation performance. SegFormer [28] was built upon a hierarchically structured Transformer encoder and a lightweight multilayer perceptron (MLP) decoder to achieve high precision and running speeds. Wan *et al.* [25] introduced an efficient squeeze-enhanced Axial Transformer (SeaFormer) to reduce the computational complexity of axial attention. Recently, Guo *et al.* [14] proposed SegNeXt to demonstrate that an encoder with simple and cheap convolutions can still achieve competitive performance.

Nevertheless, how to make the lightweight model have higher segmentation accuracy is still to be explored. Due to the limited feature representation capability, it is difficult for lightweight models to model the boundaries and categories of foreground objects, which can lead to problems such as inaccurate boundary segmentation and misclassification. To address these problems, we carefully design the Rectangular Self-Calibration Module (RCM) to improve the position modeling of foreground objects. Besides, a Dynamic Prototype Guided (DPG) head is proposed to embed class information to improve the class discrimination of foreground objects. Moreover, to further introduce the pyramid context to improve the feature representation, we design a context-guided spatial feature reconstruction network (CGRSeg), which consists of pyramid context extraction, spatial feature reconstruction, and a lightweight head.

The Rectangular Self-Calibration Module is proposed to improve the ability to locate foreground objects and extract pyramid context. The rectangular self-calibration attention is a core component of RCM. It adopts horizontal pooling and vertical pooling to capture the axial global context and generate two axis vectors. The two axis vectors are added together to model a rectangular attention region. A shape self-calibration function is designed to adjust the shape of rectangular attention and bring it closer to the foreground features, which con-

sists of large-kernel strip convolution. Besides, a fusion function is designed to fuse attention features and increase local detail. In this way, RCM can make the model focus more on the foreground for spatial feature reconstruction and can capture axial global context for pyramid context extraction.

The Dynamic Prototype Guided head is proposed to improve the classification of the foreground objects via explicit class embedding. Specifically, the features are first projected into the class feature space. And, the feature in class space and the feature in pixel space are multiplied to obtain the dynamic prototype. The dynamic prototype can reflect the feature distribution of all classes on each image. To further embed class information, the dynamic prototype is compressed to obtain the class embedding vector. Finally, the class embedding vector is projected into the pixel feature space, and the pixel features are weighted to enhance the discrimination between different classes. In this way, the DPG head can better distinguish features of different classes and improve classification performance.

The proposed CGRSeg achieves state-of-the-art segmentation performance on ADE20K, COCO Stuff, and Pascal Context with fewer FLOPs and higher Throughputs. The performance on ADE20K is shown in Figure 1. Specifically, our method achieves 43.6% mIoU on ADE20K with only 4.0 GFLOPs, which is 0.9% and 2.5% mIoU better than SeaFormer [28] and SegNeXt [14] but with about 38.0% fewer GFLOPs.

2 Related Work

Efficient Semantic Segmentation Segmentation is one of the basic tasks in computer vision. The lightweight semantic segmentation methods based on CNN include BiSeNet series [29], STDCNet [11], DFANet [18], SegNeXt [14] and so on. BiSeNet [29] first proposed a two-pathway architecture that uses a spatial path and a context path to capture both local and global information. STDCNet [11] designed a STDC module to extract scalable receptive field and multi-scale information and it uses boundary supervision to supplement spatial details. SegNeXt [14] evoked spatial attention via multi-scale convolutional features. It indicated that an encoder with simple and cheap convolutions can still perform better than vision transformers. In recent years, some Transformer-based methods have been proposed, such as SegFormer [25], TopFormer [35], and SeaFormer [25]. TopFormer [35] proposed a lightweight segmentation network based on CNN and transformer. It takes Tokens from various scales as input to produce scale-aware semantic features, which are then injected into the corresponding tokens to augment the representation. SeaFormer [25] designed a squeeze-enhanced axial Transformer in the encoder to improve feature representation and proposed a new two-path structure. It can achieve high precision with small flops. Different from these methods, our CGRSeg employed pyramid context-guided spatial feature reconstruction to improve the ability to model foreground objects, which is more efficient.

Efficient Context Extraction Modules In previous works, attention is often used for context extraction, such as coordinate attention and GatherExcite. Coordinate attention [15] captured the axial global context through horizontal and vertical pooling and extracted coordinate relationships to enhance positional awareness. GatherExcite [16] efficiently aggregated feature responses from a large spatial extent, and redistributed the pooled information to local features. The proposed RCM uses addition to model the critical region, and designs shape self-calibration to calibrate the rectangle attention, which can make the model pay more attention to the foreground features. These designs allow RCM to outperform existing attention. With the development of transformers, some convolutional networks [22, 30] adopted transformer-like structures to improve feature representation. ConvNeXt [22] first proposed the structure of large kernel depth-wise convolution combined with BN and MLP, which can significantly improve the feature representation of traditional convolutional neural networks. InceptionNeXt [30] proposed the MetaNeXt architecture and combined the Inception block with the MetaNeXt architecture to significantly improve model performance. These works show that the MetaNeXt structure has powerful context extraction ability.

Segmentation Head Segmentation heads are usually designed to improve the performance of segmentation networks. Some segmentation heads use multi-scale features to achieve advanced performance, such as PSPNet [36], DeepLab series [4–6, 21]. PSPNet [36] designed pyramid pooling model to capture multi-scale information. Some segmentation heads, such as OCRHead [31] and DA-Head [12], captured long-range dependencies to improve performance. Hamburger Head [13] is a powerful global context module based on matrix decomposition, surpassing various attention modules on semantic segmentation. However, the existing segmentation heads are not suitable for efficient semantic segmentation because of their high computational complexity.

3 Method

3.1 CGRSeg

Previous work [7, 12, 25, 35] has shown that foreground object modeling and pyramid context extraction are critical for segmentation. To this end, we design a context-guided spatial feature reconstruction network (CGRSeg). As is shown in Figure 2, CGRSeg consists of three key parts: pyramid context extraction, spatial feature reconstruction, and a lightweight head. To make the model focus on the foreground features, a Rectangular Self-Calibration Module (RCM) is proposed. Besides, it captures the axial global context for pyramid context extraction. A Dynamic Prototype Guided (DPG) head is proposed to improve the classification of the foreground objects via explicit class embedding.

Pyramid Context Extraction The RCM is applied to extract pyramid context, which applies horizontal and vertical pooling to capture axial context in two directions. Besides, RCM employs MLP to further enhance feature representation. As shown in Figure 2, a stepwise downsampling encoder is used in the

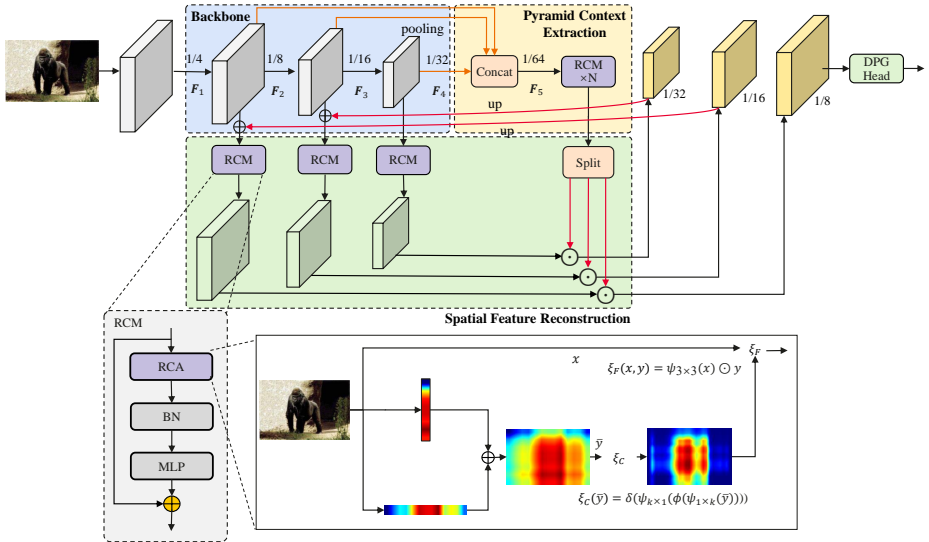


Fig. 2: The overall architecture of CGRSeg. The Rectangular Self-Calibration Module (RCM) is designed for spatial feature reconstruction and pyramid context extraction. The rectangular self-calibration attention (RCA) explicitly models the rectangular region and calibrates the attention shape. The Dynamic Prototype Guided (DPG) head is proposed to improve the classification of the foreground objects via explicit class embedding.

proposed model. Encoder produces features of different scales features as $[\mathbf{F}_1, \mathbf{F}_2, \mathbf{F}_3, \mathbf{F}_4]$, with the resolution of $[\frac{H}{4} \times \frac{W}{4}, \frac{H}{8} \times \frac{W}{8}, \frac{H}{16} \times \frac{W}{16}, \frac{H}{32} \times \frac{W}{32}]$, respectively. To ensure the efficiency of the whole network, the largest-scale feature, *i.e.*, \mathbf{F}_1 , is dropped by the decoder. Then, the lower-scale features $\mathbf{F}_2, \mathbf{F}_3$ and \mathbf{F}_4 are down-sampled to $\frac{H}{64} \times \frac{W}{64}$ size by the average pooling, and they are concatenated together to generate the pyramid feature \mathbf{F}_5 . \mathbf{F}_5 is fed into multiple stacked RCMs for pyramid feature interaction and extract scale-aware semantic features. Finally, the features are split and upsampled to the original scale after the pyramid feature extraction. This process can be formulated as:

$$P = \text{RCM}(\text{AP}(\mathbf{F}_2, 8), \text{AP}(\mathbf{F}_3, 4), \text{AP}(\mathbf{F}_4, 2)), \quad (1)$$

where $\text{AP}(\mathbf{F}, x)$ represents the operation of average pooling that down-samples the feature \mathbf{F} by the factor x . P is the feature with pyramid context.

Spatial Feature Reconstruction To make the decoder features more focused on the foreground, RCM is used to reconstruct the spatial features. Specifically, the CGRSeg fuses the low-level spatial features from the encoder with the high-level features of the corresponding scale in the decoder. The fused features are reconstructed by using RCM. RCM captures the axial global context to model the rectangular critical region, and then uses the shape self-calibration function to adjust the attention region to the foreground. Moreover, pyramid

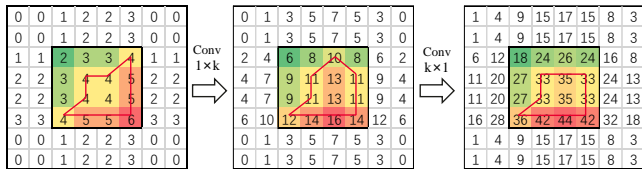


Fig. 3: The shape change of the highlighted region is caused by the rectangular self-calibration attention. By training to adjust the weights of the two strip convolutions, the attention region is calibrated closer to the foreground object.

features are applied to guide the spatial feature reconstruction to make the reconstructed features feel multi-scale information.

Dynamic Prototype Guided Head To improve the classification of foreground objects, we introduce a dynamic prototype guided segmentation head. The segmentation head generates the dynamic prototype to embed class information. The class embedding helps to enhance the distinction between different classes and improve classification accuracy.

3.2 Rectangular Self-Calibration Module

The Rectangular Self-Calibration Module (RCM) is designed to make the model focus on the foreground features. It can also capture the axial global context for pyramid context extraction. The module consists of rectangular self-calibration attention, batch normalization, and MLP.

The rectangular self-calibration attention adopts horizontal pooling and vertical pooling to capture the axial global context in two directions and uses broadcast addition to model the rectangle region of interest. Then, a shape self-calibration function is designed to calibrate the region of interest, which can make the region of interest closer to the foreground object. Here, two large-kernel strip convolutions are used to calibrate the attention map in the horizontal and vertical directions decoupledly. First, we use the horizontal strip convolution to calibrate the shape in the horizontal direction, which adjusts each row of elements to make the horizontal shape closer to the foreground object. Then, the features are normalized by BN and the non-linearity is added by ReLU. The shape is also calibrated by using the vertical strip convolution in the vertical direction. In this way, the convolution in two directions can be decoupled, which can adapt to any shape.

The weights of the strip convolutions are learnable. As shown in Figure 3, the shape of the highlighted area is changed by two strip convolutions with different weights. By training, this function can learn the appropriate weights to adjust the rectangular area to the foreground object. Furthermore, in Figure 2, the visualization results show that the rectangular self-calibration attention does effectively model the rectangular key region and adjusts the features to focus more on the foreground by the shape self-calibration function. The shape self-calibration function can be formulated as follows:

$$\xi_C(\bar{y}) = \delta(\psi_{k \times 1}(\phi(\psi_{1 \times k}(\bar{y})))) \quad (2)$$

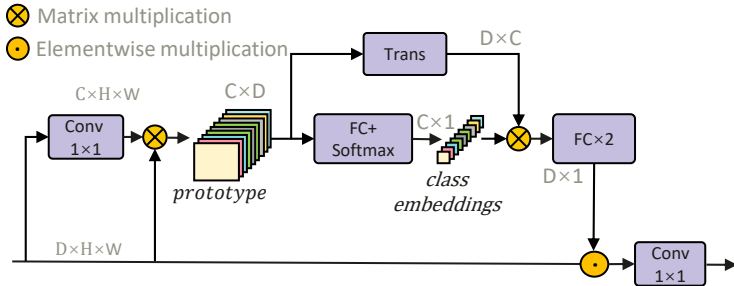


Fig. 4: Dynamic Prototype Guided Head.

where ψ indicates the large kernel strip convolution, and k indicates the kernel length of the strip convolution. ϕ indicates the Batch Normalization followed by the ReLU function, and δ indicates the Sigmoid function.

Besides, a feature fusion function is designed to fuse attention features with input features. Specifically, 3×3 depth-wise convolution is used to further extract local details of the input feature, and the calibrated attention feature is weighted to the feature by Hadamard Product.

$$\xi_F(x, y) = \psi_{3 \times 3}(x) \odot y \quad (3)$$

where $\psi_{3 \times 3}$ indicates the deep-wise convolution with kernel 3×3 . y is the attention feature obtained in the previous step. \odot is the Hadamard Product.

Recently, ConvNeXt [22] proposed the MetaNeXt structure which significantly improves the performance of convolution in the classification task. Inspired by this idea, we combine rectangular self-calibration attention with the MetaNeXt structure to further improve feature representation. Specifically, batch normalization and MLP are added after the rectangular self-calibration attention to refine features. Finally, the residual connection is employed to further enhance feature reuse. The architecture of the RCM is shown in Figure 2. It also can be described as:

$$\mathbf{F}_{\text{out}} = \rho(\xi_F(x, \xi_C(\mathbf{H}_P(x) \oplus \mathbf{V}_P(x)))) + \mathbf{F}_{\text{in}} \quad (4)$$

where \oplus indicates broadcast addition. H_P and V_P represents Horizontal Pooling and Vertical Pooling. ρ refers to BN and MLP.

3.3 Dynamic Prototype Guided Head

To improve the classification of foreground objects, the Dynamic Prototype Guided head is proposed. The DPG head generates the dynamic prototype to embed class information. The class embedding feature is projected into the pixel feature space and weight pixel features to enhance the distinction between different classes. The overall architecture of DPG Head is shown in Fig. 4.

First, we project features into the class feature space. Then, the feature in class space and the feature in pixel space are multiplied to obtain the dynamic

prototype. The dynamic prototype can reflect the feature distribution of different classes on each image, and it follows the dynamic change of the input. The process of generating the dynamic prototype can be expressed as:

$$\mathbf{F}_p = \delta_{D \rightarrow C}(\mathbf{F}_x) \otimes \mathbf{F}_x, \quad (5)$$

where \otimes is the matrix multiplication operation. \mathbf{F}_p represents the prototype.

Then, the DPG head further embedded class information to enhance the distinction between different classes. A fully connected layer is applied to compress the prototype to $C \times 1$ dimension to embed the class information and generate the class embedding vector, and Softmax is utilized to constrain the value between 0 and 1. The class embedding vector $1 \times C$ represents the global information in each class. To project the class embedding vector into the pixel feature space, we multiply the class embedding vector by the transposed prototype. With the class embedding enhancement, the new attention vector has a stronger ability to distinguish the classes. Then, two fully connected layers are used to capture the context in the attention vector. Layer Normalization is utilized to normalize features between two layers. The calculation process of the class embedding vector is summarized by:

$$\mathbf{F}_{gp} = \text{Softmax}(\delta_{D \rightarrow 1}(\mathbf{F}_p)) \quad (6)$$

where δ represents the fully connected layer.

Finally, the attention vector is weighted to pixel features to emphasize important features and enhance feature representation. The calculation of the whole process is:

$$\mathbf{F}_o = \delta(\text{ReLU}(\text{LN}(\delta(\mathbf{F}_p \otimes \mathbf{F}_{gp})))) \odot \mathbf{F}_x, \quad (7)$$

where LN and ReLU are the Layer Normalization and ReLU activation function. δ represents the fully connected layer. \odot represents the broadcast Hadamard product. The calculated feature \mathbf{F}_o is then fed into the classification convolution.

It is worth noting that the DPG Head is very lightweight. The prototype is compressed to $C \times 1$ and the broadcast Hadamard product is used to spread attention to the global feature. These operations make the computational cost of the DPG Head very low. Current popular segmentation heads, *e.g.*, OCRHead [31], are in high computation complexity. Compared with them, the proposed DPG Head is more suitable for efficient semantic segmentation.

4 Experiments

4.1 Datasets

ADE20K: The ADE20K [38] is a challenging segmentation dataset. The dataset contains more than 20,000 images from diverse environments and situations, covering 150 categories. All images are exhaustively annotated with pixel-level objects and object parts labels. It consists of 20,210/2,000/3,352 images in the training, validation, and test sets.

Table 1: Results on ADE20K. We report the performance in terms of the mIoU, FLOPs, Param, and Throughputs. The top rows, middle rows and bottom rows are tiny models, base models and large models, respectively.

Method	mIoU	FLOPs(G)	Param(M)	Thp.(Img/s)
DeeplabV3+(ECCV'18) [7]	34.0	69.4	15.4	63.0
Segformer-B0(NeurIPS'21) [28]	37.4	8.4	3.8	117.1
FeedFormer-B0(AAAI'23) [24]	39.2	7.8	4.5	110.3
SegNeXt-T(NeurIPS'22) [14]	41.1	6.6	4.3	123.5
Seaformer-L(ICLR'23) [25]	42.7	6.5	14.0	142.3
PEM-STDC1(CVPR'24) [3]	39.6	16.0	17.0	-
CGRSeg-T (Ours)	43.6	4.0	9.4	138.4
DeeplabV3+(ECCV'18) [7]	44.1	255.1	62.7	21.6
EncNet(CVPR'18) [34]	44.7	218.8	68.6	23.4
CCNet(ICCV'19) [17]	45.2	278.4	68.9	23.2
Segformer-B1(NeurIPS'21) [28]	42.2	15.9	13.7	96.0
SegNeXt-S(NeurIPS'22) [14]	44.3	15.9	13.9	91.1
FeedFormer-B1(AAAI'23) [24]	41.0	10.0	4.6	87.2
PEM-STDC2(CVPR'24) [3]	45.0	19.3	21.0	-
CGRSeg-B (Ours)	45.5	7.6	18.1	98.4
Segformer-B2(NeurIPS'21) [28]	46.5	62.4	27.5	70.4
MaskFormer(NeurIPS'21) [9]	46.7	55.0	42.0	-
Mask2Former(CVPR'22) [8]	47.7	74.0	63.0	-
FeedFormer-B2(AAAI'23) [24]	48.0	42.7	29.1	56.9
LRFormer-T(arXiv'23) [27]	46.7	17.0	13.0	-
CGRSeg-L (Ours)	48.3	14.9	35.7	73.0

COCO-Stuff: COCO-Stuff is built from COCO dataset by augmenting all 164K images with pixel-level stuff annotation. It contains 172 categories with 80 things, 91 stuff and 1 unlabeled class. There are 118K/5K/20K/20K images for training, validation, test-dev and test-challenging.

Pascal Context: The PASCAL Context dataset is an extension of the PASCAL VOC 2010 detection challenge, which contains 59 classes. The dataset contains 10100 images, including 4996 images in the training set and 5104 images in the test set.

4.2 Implementation details

Our implementation is based on the public codebase mmsegmentation [10]. We use EfficientFormerV2 [20] as the backbone network. For the ADE20K dataset, we follow SegNeXt [14] to use 160K scheduler and the batch size is 16. The initial learning rate is 0.00012 and the weight decay is 0.01. A “poly” learning rate scheduled with factor 1.0 is adopted. The training images are resized to 1024×512 for ADE20K. For the COCO-Stuff dataset, we use 80K scheduler and the batch size is 8. The initial learning rate is 0.00012 and the weight decay is 0.01. The training images are resized to 1024×512. For all three datasets, we

Table 2: Performance comparison of state-of-the-art methods on COCO-Stuff dataset.

Method	mIoU(%)	FLOPs(G)	Param(M)
SegFormer-B0 [28]	35.6	8.4	3.8
SegNeXt-T [14]	38.7	6.6	4.3
CGRSeg-T	42.2	4.0	9.4
HRFormer-S [32]	37.9	109.5	13.5
SegFormer-B1 [28]	40.2	15.9	13.7
SegNeXt-S [14]	42.2	15.9	13.9
CGRSeg-B	43.5	7.6	18.1
HRFormer-B [32]	42.4	280.0	56.2
LRFormer-T [27]	43.9	17.0	13
SegFormer-B2 [28]	44.6	62.4	27.5
SegNeXt-B [14]	45.8	34.9	27.6
CGRSeg-L	46.0	14.9	35.7

use the default data augmentation strategy in mmsegmentation. For the Pascal Context dataset, the training iteration is also 80K with batch size 16. The initial learning rate is 0.00006 and the weight decay is 0.01. The training images are resized to 480×480 .

4.3 Comparisons with the State-of-the-art Methods

Results on ADE20K. As shown in Table 1, we compare the proposed method with various state-of-the-art models on the ADE20K dataset. We report the performance of our model with three variant sizes, *i.e.*, the tiny model, the base model, and the large model.

For the tiny models, the proposed CGRSeg-T achieves 43.6% mIoU with only 4.0 GFLOPs. It performs better than all other CNN-based models and transformer-based models in terms of the mIoU and FLOPs. For example, it exceeds the previous best model SeaFormer-L by +0.9% mIoU with 2.5 GFLOPs lower computation cost and 4.6M lower parameters. As for the base models, the proposed CGRSeg-B yields 45.5% mIoU with 7.6 GFLOPs. Note the computation cost of our model is only half of the best compared SegNeXt-S (15.9 GFLOPs) model, but the performance is +1.2% mIoU better. Among the large models, our CGRSeg-L model (15.1 GFLOPs) outperforms MaskFormer (Swin-T) and Mask2Former (Swin-T) over +1.6%/+0.6% mIoU, but only with around 1/4 computational cost, which demonstrates the high efficiency of our model.

Based on the above experimental results, we can conclude that the proposed CGRSeg can achieve higher performance with less computation cost under the same experimental setup. This is because the proposed RCM can make the model focus more on the key areas and improve the feature representation. Therefore, our model can achieve high segmentation accuracy at a small computation cost.

Results on COCO-Stuff. We compare the proposed CGRSeg with previous approaches on COCO-Stuff [2] dataset in Table 2. The performance of our model

Table 3: Performance comparison of state-of-the-art methods on Pascal Context dataset. The FLOPs is calculated with the input size of 512×512. MS stands for multi-scale test setup.

Method	mIoU(MS,%)	FLOPs(G)	Param(M)
DANet [12]	52.6	277.7	69.1
EncNet [34]	52.6	-	-
EMANet [19]	53.1	246.1	53.1
SegNeXt-T [14]	53.3	6.6	4.3
CGRSeg-T	54.1	4.0	9.4
HamNet [13]	55.2	277.9	69.1
HRNet(OCR) [26]	56.2	-	74.5
HRFormer-S [32]	54.6	-	-
Senformer [1]	54.3	179.0	55.0
SegNeXt-S [14]	56.1	15.9	13.9
CGRSeg-B	56.5	7.6	18.1
Senformer [1]	56.6	199.0	79.0
CGRSeg-L	58.5	14.9	35.7

Table 4: The ablation analysis of the RCM and the DPG Head. Spatial feature reconstruction and pyramid context extraction are denoted as SFR and PCE, respectively.

RCM(SFR)	RCM(PCE)	DPG Head	mIoU(%)	FLOPs(G)	Param(M)
×	×	×	40.86	3.56	6.08
×	×	✓	41.34	3.64	6.08
×	✓	✓	42.57	3.83	9.08
✓	✓	×	42.56	3.92	9.36
✓	✓	✓	43.60	4.00	9.36

can exceed the previous best methods SegNeXt [14] with less computation cost. For example, the tiny (T), base (B), and large (L) versions of CGRSeg exceed the best-compared method by at least +3.5%, +1.3% and +0.2% mIoU with only 61%, 48%, and 43% FLOPs. In addition, CGRSeg-L outperformed LRFormer-T by 2.1% mIoU and Flops by 2.1 G.

Results on Pascal Context. We compare the proposed CGRSeg with state-of-the-art models on the Pascal Context dataset. As shown in Table 3, our approach achieves better performance than all other compared methods. For example, our CGRSeg-T model obtains 54.1% mIoU with only 4.0 GFLOPs, which is +0.8% better than SegNeXt-T [14] with 6.6% FLOPs. When compared with the larger model SegNeXt-S, our model still achieves +0.4% better mIoU with about only 48% FLOPs. Besides, CGRSeg-B also exceeds Senformer [1] 2.2% mIoU.

Table 5: Performance comparison with other advanced segmentation heads. The DPG head significantly outperforms other heads.

Head	mIoU(%)	FLOPs(G)	Param(M)
None-local	40.9	4.05	9.4
DAHead	42.6	4.05	9.4
HamHead	42.1	4.05	9.4
GC block	42.7	3.92	9.3
SE block	42.6	3.92	9.4
DPG Head	43.6	4.00	9.4

Table 6: The performance comparison of RCA and other advanced attention block. RCA significantly outperforms other attention modules without increasing Flops.

Method	mIoU(%)	FLOPs(G)	Param(M)
Self-Att	39.9	4.1	9.6
ConvNext	41.6	4.0	9.4
InceptionNext	41.6	4.0	9.3
CorrdAtt	41.5	4.0	9.9
GatherExcite	41.7	4.0	11.0
RCA(Ours)	43.6	4.0	9.4

4.4 Ablation Study

The ablation analysis of the proposed modules. The two core components of the proposed CGRSeg are the RCM and the final DPG head. To validate the effectiveness of the two components, in Table 4, we make an ablation of the RCM and DPG head. The base model is the first row of the table without any elaborate designs. The proposed RCM is used for pyramid context extraction (PCE) and spatial feature reconstruction (SFR). In base model, we replace the RCM for pyramid context extraction by a 1×1 convolution, and directly drop RCMs for feature reconstruction. DPG Head is directly dropped. As shown in the first row of the table, when not using the two modules, the performance is only 40.86% mIoU. In third row, adding the RCM for pyramid context extraction can increase the performance by 1.23% mIoU with only an extra 0.19 GFLOPs. Adding the RCM for feature reconstruction can increase the performance by 1.13% mIoU with only an extra 0.17 GFLOPs. Adding the DPG Head, *i.e.*, the second row in the table, the performance will reach 41.34% from 40.86%. When combined with the two modules, the final performance can achieve 43.60, which is 2.74% mIoU than the base model, *i.e.*, the first row of the table.

Comparison with other advanced heads. It is well known that a lightweight segmentation head is important for building an efficient segmentation framework. Thus, we elaborately design the DPG head to meet the low FLOPs and fast speed needs. Here, as shown in Table 5, the proposed DPG Head is compared with other popular and alternative segmentation heads. To get the performance of other heads, we directly experiment by replacing the DPG Head with them in the proposed CGRSeg-T. For GCHead, it is with the least

Table 7: Performance comparison with other backbone settings.

Method	Backbone	mIoU(%)	FLOPs(G)	Param(M)
SegNeXt	MSCAN-T	41.1	6.6	4.3
CGRSeg-T	MSCAN-T	42.6	5.9	9.7

Table 8: The effect of Broadcast Addition and Broadcast Multiplication on Rectangular Self-Calibration Attention Attention.

Key Area Modeling	mIoU(%)	FLOPs(G)	Param(M)
None	42.22	4.00	9.4
Mul	43.08	4.00	9.4
Add	43.61	4.00	9.4

computation cost, but the mIoU of it is poorer than our head. Compared with HamHead, our head exceeds it by 1.5% mIoU, but FLOPs drops 0.05 G. Due to the proposed efficient DPG Head, the total computation cost of the proposed CGRSeg-T in Table 1 is with only 4.0 GFLOPs but can achieve best mIoU, compared with other state-of-the-art methods. The proposed DPG Head is efficient because of the dynamic prototype guidance.

Comparisons of alternative blocks of the RCA. As shown in Table 6, we compare the performance of other alternative sub-blocks of the RCA, *e.g.*, self-attention [35], InceptionNext [30], ConvNext [22], CoordAtt Block [15] and GatherExcite [16] Block. To compare them, we directly replace the RCM with other blocks. It can be found that the proposed CGRSeg performs better than the CoordAtt Block and GatherExcite Block by increasing 2.1% and 1.9% mIoU.

Comparisons with other backbone. To further validate the sophistication of our method, we replace the backbone with MSCAN which is the backbone of SegNeXt. As shown in Table 7, CGRSeg still increases mIoU by 1.5% and FLOPs drop by 0.7G compared to SegNeXt. This shows that our CGRSeg framework is efficient and can be adapted to different backbone networks.

Comparison of addition and multiplication in RCA. As shown in Table 8, we compare the performance of Addition and Multiplication on RCA. It can be found that explicit modeling of key regions can effectively improve

Table 9: Convolution kernel selection in shape self-calibration function.

Kernel Size	mIoU(%)
None	41.27
$1 \times 5, 5 \times 1$	42.51
$1 \times 7, 7 \times 1$	43.39
$1 \times 9, 9 \times 1$	43.50
$1 \times 11, 11 \times 1$	43.61

Table 10: Convolution kernel selection for fusion functions in Rectangular Self-Calibration Attention Attention.

Local Conv	mIoU(%)
None	42.40
1×1	41.70
3×3	43.39
5×5	42.99

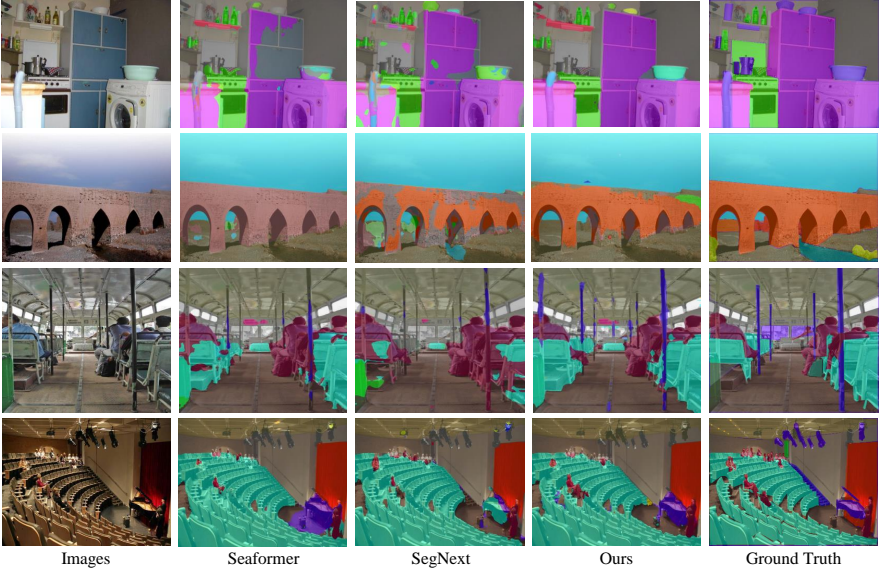


Fig. 5: Qualitative Comparison of CGRSeg-T on the ADE20K dataset.

segmentation performance. Besides, the addition performance is better than the multiplication 0.53% mIoU.

The effectiveness of the kernel size in shape self-calibration function. To investigate the effectiveness of the kernel size in the shape self-calibration function, we conduct a series of experiments in the Table 9. As the size of the convolution kernel increases, the segmentation precision also increases. When the kernel sizes are 1×11 , and 11×1 , the performance is best. Because increasing the kernel size further leads to the increase of FLOPs, we do not increase the convolution kernel. Thus, we finally choose the groups of 1×11 , and 11×1 kernel sizes in our model.

Convolution kernel selection for fusion functions in RCA. To investigate the effectiveness of the kernel size in the fusion functions, we conduct a series of experiments in the Table 10. As shown in the table, when the kernel sizes are 3×3 , the performance is best. Thus, we finally choose 3×3 kernel sizes in fusion function.

Visualization. The prediction results of SegNeXt and CGRSeg-T are visualized in Figure 5. The mask of CGRSeg is closer to the ground truth than that of other methods. It can be found that our CGRSeg-T achieves more complete segmentation masks with fewer errors. The mask is more complete because RCM can make the model pay more attention to the foreground. Besides, the DPG head can embed with category information can reduce classification errors.

5 Conclusion

In this paper, we present CGRSeg, an efficient yet competitive segmentation framework which consists of pyramid context extraction and spatial feature re-

construction. To implement these two parts, a RCM is carefully designed to make model focus on the target area and capture axial global context. Also, the DPG Head is proposed to significantly improve the feature representation with only a small amount of computation. Our CGRSeg is extensively evaluated on ADE20K, Pascal Context, and COCO-Stuff benchmarks, and achieves the state-of-the-art segmentation performance on all three datasets.

References

1. Boussselham, W., Thibault, G., Pagano, L., Machireddy, A., Gray, J., Chang, Y.H., Song, X.: Efficient self-ensemble for semantic segmentation. *British Machine Vision Conference* (2022) **11**
2. Caesar, H., Uijlings, J., Ferrari, V.: Coco-stuff: Thing and stuff classes in context. In: *CVPR*. pp. 1209–1218 (2018) **10**
3. Cavagnero, N., Rosi, G., Ruttano, C., Pistilli, F., Ciccone, M., Averta, G., Cermelli, F.: Pem: Prototype-based efficient maskformer for image segmentation. In: *Proceedings of the IEEE/CVF conference on computer vision and pattern recognition* (2024) **9**
4. Chen, L.C., Papandreou, G., Kokkinos, I., Murphy, K., Yuille, A.L.: Deeplab: Semantic image segmentation with deep convolutional nets, atrous convolution, and fully connected crfs. *IEEE T-PAMI* **40**(4), 834–848 (2017) **1, 4**
5. Chen, L.C., Papandreou, G., Schroff, F., Adam, H.: Rethinking atrous convolution for semantic image segmentation. *arXiv preprint arXiv:1706.05587* (2017) **1, 4**
6. Chen, L.C., Zhu, Y., Papandreou, G., Schroff, F., Adam, H.: Encoder-decoder with atrous separable convolution for semantic image segmentation. In: *ECCV*. pp. 801–818 (2018) **1, 4**
7. Chen, L.C., Zhu, Y., Papandreou, G., Schroff, F., Adam, H.: Encoder-decoder with atrous separable convolution for semantic image segmentation. In: *Proceedings of the European conference on computer vision (ECCV)*. pp. 801–818 (2018) **4, 9**
8. Cheng, B., Misra, I., Schwing, A.G., Kirillov, A., Girdhar, R.: Masked-attention mask transformer for universal image segmentation. In: *Proceedings of the IEEE/CVF conference on computer vision and pattern recognition*. pp. 1290–1299 (2022) **9**
9. Cheng, B., Schwing, A., Kirillov, A.: Per-pixel classification is not all you need for semantic segmentation. *NeurIPS* **34**, 17864–17875 (2021) **9**
10. Contributors, M.: MMSegmentation: Openmmlab semantic segmentation toolbox and benchmark. <https://github.com/open-mmlab/mms Segmentation> (2020) **9**
11. Fan, M., Lai, S., Huang, J., Wei, X., Chai, Z., Luo, J., Wei, X.: Rethinking bisenet for real-time semantic segmentation. In: *CVPR*. pp. 9716–9725 (2021) **3**
12. Fu, J., Liu, J., Tian, H., Li, Y., Bao, Y., Fang, Z., Lu, H.: Dual attention network for scene segmentation. In: *CVPR*. pp. 3146–3154 (2019) **4, 11**
13. Geng, Z., Guo, M.H., Chen, H., Li, X., Wei, K., Lin, Z.: Is attention better than matrix decomposition? *arXiv preprint arXiv:2109.04553* (2021) **4, 11**
14. Guo, M.H., Lu, C.Z., Hou, Q., Liu, Z.N., Cheng, M.M., Hu, S.m.: Segnext: Rethinking convolutional attention design for semantic segmentation. In: *NeurIPS* (2022) **2, 3, 9, 10, 11**
15. Hou, Q., Zhou, D., Feng, J.: Coordinate attention for efficient mobile network design. In: *Proceedings of the IEEE/CVF conference on computer vision and pattern recognition*. pp. 13713–13722 (2021) **4, 13**

16. Hu, J., Shen, L., Albanie, S., Sun, G., Vedaldi, A.: Gather-excite: Exploiting feature context in convolutional neural networks. *Advances in neural information processing systems* **31** (2018) [4](#), [13](#)
17. Huang, Z., Wang, X., Huang, L., Huang, C., Wei, Y., Liu, W.: Ccnet: Criss-cross attention for semantic segmentation. In: *ICCV*. pp. 603–612 (2019) [9](#)
18. Li, H., Xiong, P., Fan, H., Sun, J.: Dfanet: Deep feature aggregation for real-time semantic segmentation. In: *CVPR*. pp. 9522–9531 (2019) [3](#)
19. Li, X., Zhong, Z., Wu, J., Yang, Y., Lin, Z., Liu, H.: Expectation-maximization attention networks for semantic segmentation. In: *Proceedings of the IEEE/CVF International Conference on Computer Vision*. pp. 9167–9176 (2019) [11](#)
20. Li, Y., Hu, J., Wen, Y., Evangelidis, G., Salahi, K., Wang, Y., Tulyakov, S., Ren, J.: Rethinking vision transformers for mobilenet size and speed. *arXiv preprint arXiv:2212.08059* (2022) [9](#)
21. Liu, C., Chen, L.C., Schroff, F., Adam, H., Hua, W., Yuille, A.L., Fei-Fei, L.: Auto-deeplab: Hierarchical neural architecture search for semantic image segmentation. In: *CVPR*. pp. 82–92 (2019) [1](#), [4](#)
22. Liu, Z., Mao, H., Wu, C.Y., Feichtenhofer, C., Darrell, T., Xie, S.: A convnet for the 2020s. In: *CVPR*. pp. 11976–11986 (2022) [4](#), [7](#), [13](#)
23. Long, J., Shelhamer, E., Darrell, T.: Fully convolutional networks for semantic segmentation. In: *CVPR*. pp. 3431–3440 (2015) [1](#)
24. Shim, J.h., Yu, H., Kong, K., Kang, S.J.: Feedformer: Revisiting transformer decoder for efficient semantic segmentation. In: *Proceedings of the AAAI Conference on Artificial Intelligence*. vol. 37, pp. 2263–2271 (2023) [9](#)
25. Wan, Q., Huang, Z., Lu, J., Yu, G., Zhang, L.: Seaformer: Squeeze-enhanced axial transformer for mobile semantic segmentation (2023) [1](#), [2](#), [3](#), [4](#), [9](#)
26. Wang, J., Sun, K., Cheng, T., Jiang, B., Deng, C., Zhao, Y., Liu, D., Mu, Y., Tan, M., Wang, X., Liu, W., Xiao, B.: Deep high-resolution representation learning for visual recognition. *TPAMI* (2019) [11](#)
27. Wu, Y.H., Zhang, S.C., Liu, Y., Zhang, L., Zhan, X., Zhou, D., Feng, J., Cheng, M.M., Zhen, L.: Low-resolution self-attention for semantic segmentation. *arXiv preprint arXiv:2310.05026* (2023) [9](#), [10](#)
28. Xie, E., Wang, W., Yu, Z., Anandkumar, A., Alvarez, J.M., Luo, P.: Segformer: Simple and efficient design for semantic segmentation with transformers. *NeurIPS* **34**, 12077–12090 (2021) [1](#), [2](#), [3](#), [9](#), [10](#)
29. Yu, C., Wang, J., Peng, C., Gao, C., Yu, G., Sang, N.: Bisenet: Bilateral segmentation network for real-time semantic segmentation. In: *ECCV*. pp. 325–341 (2018) [2](#), [3](#)
30. Yu, W., Zhou, P., Yan, S., Wang, X.: Inceptionnext: When inception meets convnext. *arXiv preprint arXiv:2303.16900* (2023) [4](#), [13](#)
31. Yuan, Y., Chen, X., Wang, J.: Object-contextual representations for semantic segmentation. In: *ECCV*. pp. 173–190 (2020) [4](#), [8](#)
32. Yuan, Y., Fu, R., Huang, L., Lin, W., Zhang, C., Chen, X., Wang, J.: Hrformer: High-resolution vision transformer for dense predict. *NeurIPS* **34**, 7281–7293 (2021) [10](#), [11](#)
33. Zhang, B., Tian, Z., Tang, Q., Chu, X., Wei, X., Shen, C., et al.: Segvit: Semantic segmentation with plain vision transformers pp. 4971–4982 (2022) [1](#)
34. Zhang, H., Dana, K., Shi, J., Zhang, Z., Wang, X., Tyagi, A., Agrawal, A.: Context encoding for semantic segmentation. In: *CVPR*. pp. 7151–7160 (2018) [9](#), [11](#)
35. Zhang, W., Huang, Z., Luo, G., Chen, T., Wang, X., Liu, W., Yu, G., Shen, C.: Top-former: Token pyramid transformer for mobile semantic segmentation. In: *CVPR*. pp. 12083–12093 (2022) [3](#), [4](#), [13](#)

36. Zhao, H., Shi, J., Qi, X., Wang, X., Jia, J.: Pyramid scene parsing network. In: CVPR. pp. 2881–2890 (2017) [1](#), [4](#)
37. Zheng, S., Lu, J., Zhao, H., Zhu, X., Luo, Z., Wang, Y., Fu, Y., Feng, J., Xiang, T., Torr, P.H., et al.: Rethinking semantic segmentation from a sequence-to-sequence perspective with transformers. In: CVPR. pp. 6881–6890 (2021) [1](#)
38. Zhou, B., Zhao, H., Puig, X., Fidler, S., Barriuso, A., Torralla, A.: Scene parsing through ade20k dataset. In: CVPR. pp. 633–641 (2017) [2](#), [8](#)